Search for $\eta_c(2S) \to \pi^+\pi^-\eta_c$ and $\eta_c(2S) \to \pi^+\pi^- K_S^0 K^\pm \pi^\mp$ decays

M. Ablikim *et al.*[*]
(BESIII Collaboration)

(Received 10 January 2024; accepted 21 March 2024; published 29 April 2024)

Based on $(27.12 \pm 0.14) \times 10^8$ $\psi(2S)$ events collected by the BESIII detector, we search for the decay $\eta_c(2S) \to \pi^+\pi^-\eta_c$ via $\psi(2S) \to \gamma\eta_c(2S)$. No significant signal is observed, and the upper limit on the product branching fraction $\mathcal{B}(\psi(2S) \to \gamma\eta_c(2S)) \times \mathcal{B}(\eta_c(2S) \to \pi^+\pi^-\eta_c)$ is determined to be 2.21×10^{-5} at the 90% confidence level. In addition, the $\eta_c(2S) \to \pi^+\pi^- K_S^0 K^\pm \pi^\mp$ decay is studied via $\psi(2S) \to \gamma\eta_c(2S)$ and is observed with a statistical significance of 10σ for the first time. The branching fraction of $\eta_c(2S) \to \pi^+\pi^- K_S^0 K^\pm \pi^\mp$ is determined to be $(1.33 \pm 0.11 \pm 0.40 \pm 0.95) \times 10^{-2}$, where the first uncertainty is statistical, the second is systematic, and the third uncertainty is due to the quoted $\mathcal{B}(\psi(2S) \to \gamma\eta_c(2S))$.

DOI: 10.1103/PhysRevD.109.072017

I. INTRODUCTION

Studies of decays of charmonium states play an important role in understanding the strong interaction. Although the charmonium states J/ψ and $\psi(2S)$ have been observed for more than half a century, intensive studies of different decays of various charmonium states are still highly desirable, especially for the spin singlet sector [1], which includes the $^1P_1$ state h_c and the 2^1S_0 state $\eta_c(2S)$. The $\eta_c(2S)$ is the first excited state of the pseudoscalar ground state η_c, lying just below the mass of its vector counterpart, $\psi(2S)$ [1]. It was first observed by Belle [2] in the process $B^\pm \to K^\pm\eta_c(2S)$ with $\eta_c(2S) \to K_S^0 K^\pm\pi^\mp$, and was subsequently confirmed and studied by *BABAR* [3], CLEO [4] and Belle [5] in the $\gamma\gamma$-fusion to the $K\bar{K}\pi$ final state, by *BABAR* [6] in the double charmonium production process $e^+e^- \to J/\psi c\bar{c}$, by Belle [7] in the inclusive process $e^+e^- \to J/\psi +$anything, and by BESIII in the decay $\psi(2S) \to \gamma\eta_c(2S)$ [8].

Hadronic transitions between charmonium states offer a good platform to study the dynamics of heavy quarks. Experimental [9] and theoretical [10,11] investigations of these transitions have provided a comprehensive understanding of those processes involving the emission of two-pion system within the framework of low-energy chiral dynamics. Such decays are usually described as heavy quarkonium transitions generating a soft gluonic field which then produces the light mesons in QCD picture, as shown in Fig. 1. However, the two-pion transition between the $^1S_0$ charmonium states has not yet been observed.

The transition amplitude of the $\eta_c(2S) \to \pi^+\pi^-\eta_c$ decay [12] is expected to exhibit the same linear dependence q^2 as the $\psi(2S) \to \pi^+\pi^- J/\psi$ decay [13], where q is the total 4-momentum of the pion pair. With the single-channel approach, the branching fraction of $\eta_c(2S) \to \pi^+\pi^-\eta_c$ is estimated to be ~5% [12,14]. However, this decay branching fraction may be suppressed due to the contribution of the chromo-magnetic interaction in its decay amplitude [15]. A previous study indicated that the $\eta_c(2S) \to \pi^+\pi^-\eta_c$ decay may be the most promising decay mode of the $\eta_c(2S)$ [12]. The *BABAR* Collaboration set the upper limit on its decay branching fraction at the 90% confidence level (CL) to be 7.4%, based on e^+e^- collision data corresponding to an integrated luminosity of (429.1 ± 1.9) fb^{-1} collected at the $\Upsilon(4S)$ resonance [16]. In recent years, the BESIII Collaboration collected a large $\psi(2S)$ data sample, which provides a great opportunity to search for $\eta_c(2S) \to \pi^+\pi^-\eta_c$ and thereby test different theoretical calculations [10,11].

In addition, only a few decay modes of $\eta_c(2S)$ have been observed to date. Searching for new decay modes of $\eta_c(2S)$ is important to deeply understand its decay properties. Using 106 million $\psi(2S)$ events collected by the BESIII detector, evidence for the decay $\eta_c(2S) \to \pi^+\pi^- K_S^0 K^\pm\pi^\mp$ was found with statistical significance of 4.2σ [17]. With $(27.12 \pm 0.14) \times 10^8$ $\psi(2S)$ events taken by the BESIII detector, which is about 25 times larger than the previous data sample [17], we search for $\eta_c(2S) \to \pi^+\pi^-\eta_c$ and present an improved measurement of the branching fraction of $\eta_c(2S) \to \pi^+\pi^- K_S^0 K^\pm\pi^\mp$.

[*]Full author list given at end of the article.

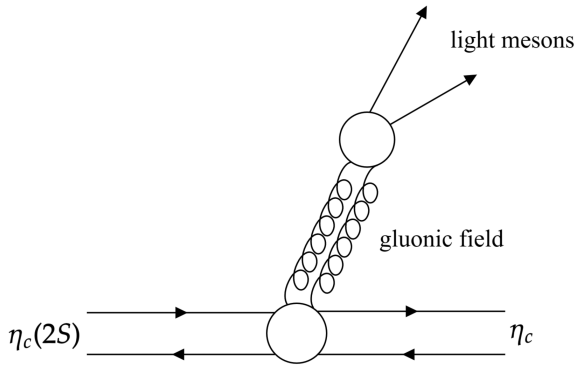

FIG. 1. The Feynman diagram for the process of $\eta_c(2S) \to \pi^+\pi^-\eta_c$.

II. BESIII DETECTOR AND MONTE CARLO SIMULATION

The BESIII detector [18] records symmetric e^+e^- collisions provided by the BEPCII storage ring [19] in the center-of-mass energy range from 2.0 to 4.95 GeV, with a peak luminosity of 1×10^{33} cm^{-2} s^{-1} achieved at $\sqrt{s} = 3.77$ GeV. BESIII has collected large data samples in this energy region [20,21]. The cylindrical core of the BESIII detector consists of a helium-based main drift chamber (MDC), a plastic scintillator time-of-flight (TOF) system, and a CsI(Tl) electromagnetic calorimeter (EMC), which are all enclosed in a super conducting solenoidal magnet providing a 1.0 T magnetic field. The solenoid is supported by an octagonal flux-return yoke with resistive plate counter modules interleaved with steel for muon identification. The acceptance for charged particles and photons is 93% of the full solid angle, and the charged-particle momentum resolution at 1 GeV/c is 0.5%. The photon energy resolution is 2.5% (5%) at 1.0 GeV in the barrel (end cap) region. The time resolution in the TOF barrel region is 68 ps, while that in the end-cap region was 110 ps. The end-cap TOF system was upgraded in 2015 using multigap resistive plate chamber technology, providing a time resolution of 60 ps, which benefits ~84% of the data used in this analysis [22–24].

Simulated data samples produced with a GEANT4-based Monte Carlo (MC) package [25], which includes the geometric description of the BESIII detector and the detector response, are used to determine detection efficiencies and to estimate backgrounds. The simulation models the beam-energy spread and initial-state radiation (ISR) in e^+e^- annihilations with the generator KKMC [26,27]. An inclusive MC sample of 2.7 billion $\psi(2S)$ events is used to investigate potential background. The inclusive MC sample includes the production of the $\psi(2S)$ resonance, the ISR production of the J/ψ, and the continuum processes incorporated in KKMC. The known particle decays are modeled with EVTGEN [28,29] using branching fractions taken from the Particle Data Group (PDG) [14], while the remaining unknown decays are estimated with LUNDCHARM [30,31].

To estimate the signal selection efficiency, detector resolution and background, several exclusive MC samples are generated. Specific generators are employed for the decays $\psi(2S) \to \gamma\eta_c(2S)$ and $\psi(2S) \to \gamma\chi_{c1,2}$, which are based on specialized models that have been packaged and customized specifically for the BESIII detector. The polar angle (θ_γ) of the radiation photon in the rest frame of $\psi(2S)$ follows $(1 + \lambda\cos^2\theta_\gamma)$ function, where the λ is 1 for $\eta_c(2S)$, $-1/3$ for χ_{c1} and $1/13$ for χ_{c2} [32]. Two decay modes $\eta_c \to K^+K^-\pi^0$ and $\eta_c \to K^0_S K^\pm\pi^\mp$ are generated according to the Dalitz plot measured by BESIII [33]. The exclusive MC samples $\psi(2S) \to \gamma\pi^+\pi^-K^+K^-\pi^0$ $(\gamma\pi^+\pi^-K^0_S K^\pm\pi^\mp)$, $\psi(2S) \to \pi^0\pi^+\pi^-K^+K^-\pi^0$ $(\pi^0\pi^+\pi^-K^0_S K^\pm\pi^\mp)$, $\psi(2S) \to (\gamma_{\rm FSR})\pi^+\pi^-K^+K^-\pi^0$ $((\gamma_{\rm FSR})\pi^+\pi^-K^0_S K^\pm\pi^\mp)$ ($\gamma_{\rm FSR}$ stands for a photon from final state radiation), are generated uniformly in the phase space.

The data sample collected at the center-of-mass energies of $\sqrt{s} = 3.650$ GeV, corresponding to an integrated luminosity of 410 pb^{-1}, is used to estimate the continuum background contribution.

III. SEARCH FOR $\eta_c(2S) \to \pi^+\pi^-\eta_c$

A. Event selection

To search for $\eta_c \to \pi^+\pi^-\eta_c$, we select the candidate events for $\psi(2S) \to \gamma\eta_c(2S)$ with $\eta_c(2S) \to \pi^+\pi^-\eta_c$, where the η_c is reconstructed with the final states of $K^+K^-\pi^0$ and $K^0_S K^\pm\pi^\mp$, where K^0_S (π^0) candidates are reconstructed with pairs of $\pi^+\pi^-$ ($\gamma\gamma$).

Charged tracks are reconstructed in the MDC using good helix fits, and are required to satisfy $|\cos\theta| < 0.93$, where θ is the polar angle with respect to the z-axis which is the symmetry axis of the MDC. For charged tracks apart from those from K^0_S decays, the distance of the closest approach to the interaction point must be less than 10 cm along the z-axis, and less than 1 cm in the transverse plane. By combining the dE/dx and TOF information, the $\chi^2_{\rm PID}(i)$ ($i = K$, π, or p) is calculated for each charged track for each hadron i hypothesis.

Photon candidates are identified using showers in the EMC. The deposited energy of each shower must be greater than 25 MeV in the barrel region ($|\cos\theta| < 0.80$) and in the end-cap region ($0.86 < |\cos\theta| < 0.92$). To reduce electronic noise and showers unrelated to the event, the difference between the EMC time and the event start time is required to be within [0, 700] ns. The angle subtended by the EMC shower and the position of the closest extrapolated charged track at the EMC must be greater than 10 degrees. Candidate events must have at least three and one good photons for the decay modes $\eta_c \to K^+K^-\pi^0$ and $\eta_c \to K^0_S K^\pm\pi^\mp$, respectively.

The π^0 candidates are selected with the invariant mass of the $\gamma\gamma$ pair satisfying $|M(\gamma\gamma) - m_{\pi^0}| < 0.015$ GeV/c^2, where $M(\gamma\gamma)$ is the invariant mass of $\gamma\gamma$ and m_{π^0} is the nominal π^0 mass [14]. To improve the momentum resolution, a one-constraint (1C) kinematic fit with $M(\gamma\gamma)$ being constrained to m_{π^0} is performed. A kinematic constraint between the production and decay vertices, and a second vertex fit algorithm based on the least square method are employed for K^0_S candidates. The K^0_S candidates must have a decay length more than 2 standard deviations of the vertex resolution away from the interaction point, and have invariant mass within 0.02 GeV/c^2 around the nominal K^0_S mass [14]. Events with $|M(K^+K^-\pi^0(K^0_SK^\pm\pi^\mp)) - m_{\eta_c}| < 0.05$ GeV/c^2 are selected for further analysis, where $M(K^+K^-\pi^0(K^0_SK^\pm\pi^\mp))$ is the invariant mass of $K^+K^-\pi^0(K^0_SK^\pm\pi^\mp)$ and m_{η_c} is the nominal η_c mass [14].

For the process of $\eta_c(2S) \to \pi^+\pi^-\eta_c$, $\eta_c \to K^+K^-\pi^0$, a kinematic fit with five constraints (5C) is performed, where the total energy-momentum of final states is constrained to the initial energy-momentum constraint (4C) and an additional constraint which constrains $M(\gamma\gamma)$ to m_{π^0}. For the process of $\eta_c(2S) \to \pi^+\pi^-\eta_c, \eta_c \to K^0_SK^\pm\pi^\mp$, a 4C kinematic fit is performed. The $\chi^2_{\rm 5C} < 25$ and $\chi^2_{\rm 4C} < 40$ are further required for the decay modes $\eta_c \to K^+K^-\pi^0$ and $\eta_c \to K^0_SK^\pm\pi^\mp$, respectively. These requirements are determined by optimizing the figure-of-merit (FOM) $S/\sqrt{S+B}$ [34], where S is the number of events from signal MC sample, and B is the number of background events estimated from the left-hand sideband region of η_c (defined as $[2.8, 2.9]$ GeV/c^2) in data.

For each event, if there are multiple combinations satisfying the above criteria, only the combination with the minimum value of $\chi^2_{\rm tot} = \chi^2_{\rm 4C} + \chi^2_{\rm 1C} + \chi^2_{\rm PID} + \chi^2_{\rm vertex}$ is kept for further analysis. Here, $\chi^2_{\rm 4C}$ is from the 4C kinematic fit, $\chi^2_{\rm 1C}$ is from the 1C kinematic fit for $\pi^0 \to \gamma\gamma$ and only applies for $\eta_c \to K^+K^-\pi^0$, $\chi^2_{\rm PID}$ is the sum of the $\chi^2_{\rm PID}(i)$ for each charged track in the event, and $\chi^2_{\rm vertex}$ is from the K^0_S second vertex fit and only applies for $\eta_c \to K^0_SK^\pm\pi^\mp$.

The background events from the $\psi(2S) \to \pi^+\pi^- J/\psi$ process are suppressed by requiring the recoil mass of $\pi^+\pi^-$ to be less than 3.07 GeV/c^2. The background events from $\psi(2S) \to \omega K^+K^-$ for the $\eta_c(2S) \to \pi^+\pi^-\eta_c$, $\eta_c \to K^+K^-\pi^0$ decay are excluded by requiring $|M(\pi^0\pi^+\pi^-) - m_\omega| > 0.02$ GeV/c^2, where $M(\pi^0\pi^+\pi^-)$ is the invariant mass of $\pi^0\pi^+\pi^-$ and m_ω is the nominal ω mass [14].

B. Background analysis

The potential backgrounds from $\psi(2S)$ decays and continuum production are studied by analyzing the $\psi(3686)$ inclusive MC sample and the continuum data at $\sqrt{s} = 3.650$ GeV, respectively. Detailed MC studies show that the background events for the $\eta_c(2S) \to \pi^+\pi^-\eta_c$, $\eta_c \to K^+K^-\pi^0$ process mainly come from $\psi(2S) \to (\gamma_{\rm FSR})\pi^+\pi^-K^+K^-\pi^0$; $\psi(2S) \to \gamma\eta_c(2S)$, $\eta_c(2S) \to \pi^+\pi^-K^+K^-\pi^0$; $\psi(2S) \to \gamma\chi_{c2}$, $\chi_{c2} \to \pi^+\pi^-K^+K^-\pi^0$, and $\psi(2S) \to \pi^0\pi^0\pi^+\pi^-K^+K^-$; and the background events for the $\eta_c(2S) \to \pi^+\pi^-\eta_c$, $\eta_c \to K^0_SK^\pm\pi^\mp$ process mainly come from $\psi(2S) \to (\gamma_{\rm FSR})\pi^+\pi^-K^0_SK^\pm\pi^\mp$, $\psi(2S) \to \gamma\eta_c(2S)$, $\eta_c(2S) \to \pi^+\pi^-K^0_SK^\pm\pi^\mp$, and $\psi(2S) \to \gamma\chi_{c2}, \chi_{c2} \to \pi^+\pi^-K^0_SK^\pm\pi^\mp$. In addition, the background events from continuum production and those from $\psi(2S)$ decays due to misidentification between charged pions and kaons are negligible. Other background events from $\psi(2S)$ decays have the same final states as the signal and form smooth shapes in the distribution of $\pi^+\pi^-K^+K^-\pi^0$ or $\pi^+\pi^-K^0_SK^\pm\pi^\mp$ invariant mass, denoted hereafter as $M(\pi^+\pi^-K^+K^-\pi^0)$ or $M(\pi^+\pi^-K^0_SK^\pm\pi^\mp)$.

The background events from $\psi(2S) \to \pi^+\pi^-K^+K^-\pi^0$ and $\psi(2S) \to \pi^+\pi^-K^0_SK^\pm\pi^\mp$, either with a fake photon or a real soft FSR photon, form a peak near the $\eta_c(2S)$ signal in the $M(\pi^+\pi^-K^+K^-\pi^0)$ or $M(\pi^+\pi^-K^0_SK^\pm\pi^\mp)$ distribution. This peak will be shifted to higher mass region, if the energy of the transition photon candidate is not involved in the 4C kinematic fit [8]. In this case, the 4C kinematic fit becomes a three-constraint (3C) kinematic fit. The MC simulation shows that the 3C kinematic fit has a similar mass resolution as the 4C kinematic fit, but with better signal-background separation, as shown in Fig. 2. Therefore the four-momenta of daughter particles updated by the 3C kinematic fit are used for further analysis. The numbers of the FSR and non-FSR events, $N_{\rm FSR}$ and $N_{\rm nonFSR}$, are connected via a ratio defined as

$$R_{\rm FSR} = \frac{N_{\rm FSR}}{N_{\rm nonFSR}}. \quad (1)$$

A correction factor $f_{\rm corr} = R^{\rm data}_{\rm FSR}/R^{\rm MC}_{\rm FSR} = 1.62 \pm 0.13$, estimated with the control sample of $\psi(2S) \to \gamma\chi_{c0}$,

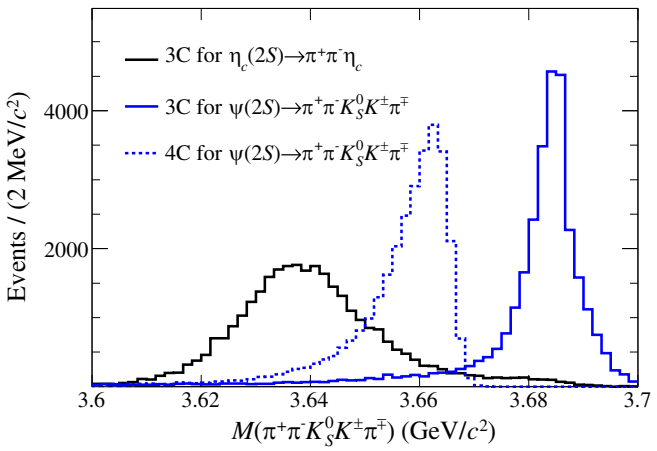

FIG. 2. Distributions of $M(\pi^+\pi^-K^0_SK^\pm\pi^\mp)$ for $\eta_c(2S) \to \pi^+\pi^-\eta_c, \eta_c \to K^0_SK^\pm\pi^\mp$ with 3C kinematic fit (black solid line), $\psi(2S) \to \pi^+\pi^-K^0_SK^\pm\pi^\mp$ with 3C kinematic fit (blue solid line) and 4C kinematic fit (blue dashed line) based on MC simulation.

$\chi_{c0} \to 3(\pi^+\pi^-)(\gamma_{\rm FSR})$, is fixed in data analysis to account for the difference in $R_{\rm FSR}$ for the background events of $\psi(2S) \to (\gamma_{\rm FSR})\pi^+\pi^- K^+K^-\pi^0$ and $\psi(2S) \to (\gamma_{\rm FSR})\pi^+\pi^- K^0_S K^\mp\pi^\mp$ between data and MC simulation [35].

In addition, the numbers of peaking background events from $\psi(2S) \to \gamma\eta_c(2S), \eta_c(2S) \to \pi^+\pi^- K^+K^-\pi^0$ and $\eta_c(2S) \to \pi^+\pi^- K^0_S K^\pm\pi^\mp$ are estimated by

$$N^{\rm peak}_{\rm bkg} = N_{\psi(2S)} \times \mathcal{B}_1 \times \mathcal{B}_2 \times \eta, \tag{2}$$

where $N_{\psi(2S)}$ is the total number of $\psi(2S)$ events, η is the misidentification rate based on MC simulation, and $\mathcal{B}_1$ is the branching fraction of $\psi(2S) \to \gamma\eta_c(2S)$ quoted from the PDG [14]. $\mathcal{B}_2$ is the branching fraction of the $\eta_c(2S)$ decay, which is $(1.4 \pm 1.0) \times 10^{-2}$ for $\eta_c(2S) \to \pi^+\pi^- K^+K^-\pi^0$ cited from the PDG [14], and $(1.33 \pm 1.04) \times 10^{-2}$ for $\eta_c(2S) \to \pi^+\pi^- K^0_S K^\pm\pi^\mp$, as discussed in Sec. IV. Finally, we obtain $N^{\rm peak}_{\rm bkg}$ to be 54 ± 39 for $\eta_c(2S) \to \pi^+\pi^- K^+K^-\pi^0$ and 122 ± 36 for $\eta_c(2S) \to \pi^+\pi^- K^0_S K^\pm\pi^\mp$.

C. Signal yield

The number of signal events of $\eta_c(2S) \to \pi^+\pi^-\eta_c$ is determined from a simultaneous unbinned maximum likelihood fit on the $M(\pi^+\pi^- K^+K^-\pi^0)$ and $M(\pi^+\pi^- K^0_S K^\pm\pi^\mp)$ distributions.

In the fit, the shape of the $\eta_c(2S)$ signal is described as

$$(E^3_\gamma \times BW(m) \times f_d(E_\gamma)) \otimes F_{\rm res} \times \varepsilon(m), \tag{3}$$

where m is $M(\pi^+\pi^- K^+K^-\pi^0)$ or $M(\pi^+\pi^- K^0_S K^\pm\pi^\mp)$, $E_\gamma = \frac{m^2_{\psi(2S)} - m^2}{2m_{\psi(2S)}}$ is the energy of the transition photon in the rest frame of $\psi(2S)$, $BW(m)$ is the Breit-Wigner function for $\eta_c(2S)$. The mass and width of $\eta_c(2S)$ are fixed to 3643.4 MeV/c^2 and 19.80 MeV, respectively, which are taken from the previous BESIII measurement [35]. The function $f_d(E_\gamma)$ is designed to damp the divergent tail raised by E^3_γ [36],

$$f_d(E_\gamma) = \frac{E^2_0}{E_\gamma E_0 + (E_\gamma - E_0)^2}. \tag{4}$$

Here, $E_0 = \frac{m^2_{\psi(2S)} - m^2_{\eta_c(2S)}}{2m_{\psi(2S)}}$. $\varepsilon(m)$ is the mass dependent efficiency function estimated by MC simulation. $F_{\rm res}$ is a double Gaussian function describing the detector resolution. The selected shapes and the nature of yields of different background components are summarized in Table I.

The fit results are shown in Fig. 3. The fit qualities are $\chi^2/{\rm ndf}_{\pi^+\pi^- K^+K^-\pi^0} = 1.59$ and $\chi^2/{\rm ndf}_{\pi^+\pi^- K^0_S K^\pm\pi^\mp} = 1.26$, where ndf is the number of degrees of freedom. No significant $\eta_c(2S)$ signal is observed from this fit.

D. Upper limit on branching fraction

The product branching fraction of $\mathcal{B}(\psi(2S) \to \gamma\eta_c(2S)) \times \mathcal{B}(\eta_c(2S) \to \pi^+\pi^-\eta_c)$ is calculated as

$$\mathcal{B} = \frac{N_{\rm sig}}{N_{\psi(2S)} \times (\varepsilon_3 \times \mathcal{B}_3 + \varepsilon_4 \times \mathcal{B}_4)}. \tag{5}$$

Here, $N_{\rm sig}$ is the upper limit on the signal yield, $\mathcal{B}_3$ ($\mathcal{B}_4$) is the branching fraction of $\eta_c \to K^+K^-\pi^0$ ($\eta_c \to K^0_S K^\pm\pi^\mp$), and ε_3 (ε_4) is the corresponding efficiency obtained with MC simulation. Due to no significant signal being observed, the upper limit on the product branching fraction

TABLE I. The selected shapes and the nature of yields of different background sources for $\eta_c(2S) \to \pi^+\pi^-\eta_c$. All simulated shapes are derived from individual exclusive MC samples. '⊗ Gaussian' denotes that the simulated shapes are smeared with a Gaussian function with parameters obtained from the corresponding χ_{cJ} signal. The parameters of the Chebyshev polynomial function are free.

$\eta_c(2S) \to \pi^+\pi^-\eta_c, \eta_c \to K^+K^-\pi^0$			
No.	Source	Shape	Nature of yield
I	$\psi(2S) \to \gamma\eta_c(2S), \eta_c(2S) \to \pi^+\pi^- K^+K^-\pi^0$	Eq. (3)	Fixed at $N^{\rm peak}_{\rm bkg}$ (See Sec. III B)
II	$\psi(2S) \to \gamma\chi_{c2}, \chi_{c2} \to \pi^+\pi^- K^+K^-\pi^0$	Simulated shape ⊗ Gaussian	Floated
III	$\psi(2S) \to (\gamma_{\rm FSR})\pi^+\pi^- K^+K^-\pi^0$	Simulated shape ⊗ Gaussian	Floated
IV	$\psi(2S) \to \pi^0\pi^+\pi^-\eta_c, \eta_c \to K^+K^-\pi^0$	Simulated shape	Floated
V	$\psi(2S) \to \gamma\pi^+\pi^- K^+K^-\pi^0$	The third-order Chebyshev function	Floated

$\eta_c(2S) \to \pi^+\pi^-\eta_c, \eta_c \to K^0_S K^\pm\pi^\mp$			
No.	Source	Shape	Nature of yield
I	$\psi(2S) \to \gamma\eta_c(2S), \eta_c(2S) \to \pi^+\pi^- K^0_S K^\pm\pi^\mp$	Eq. (3)	Fixed at $N^{\rm peak}_{\rm bkg}$ (See Sec. III B)
II	$\psi(2S) \to \gamma\chi_{c2}, \chi_{c2} \to \pi^+\pi^- K^+K^-\pi^0$	Simulated shape ⊗ Gaussian	Floated
III	$\psi(2S) \to (\gamma_{\rm FSR})\pi^+\pi^- K^0_S K^\pm\pi^\mp$	Simulated shape ⊗ Gaussian	Floated
IV	$\psi(2S) \to \gamma\pi^+\pi^- K^0_S K^\pm\pi^\mp$	Simulated shape	Floated

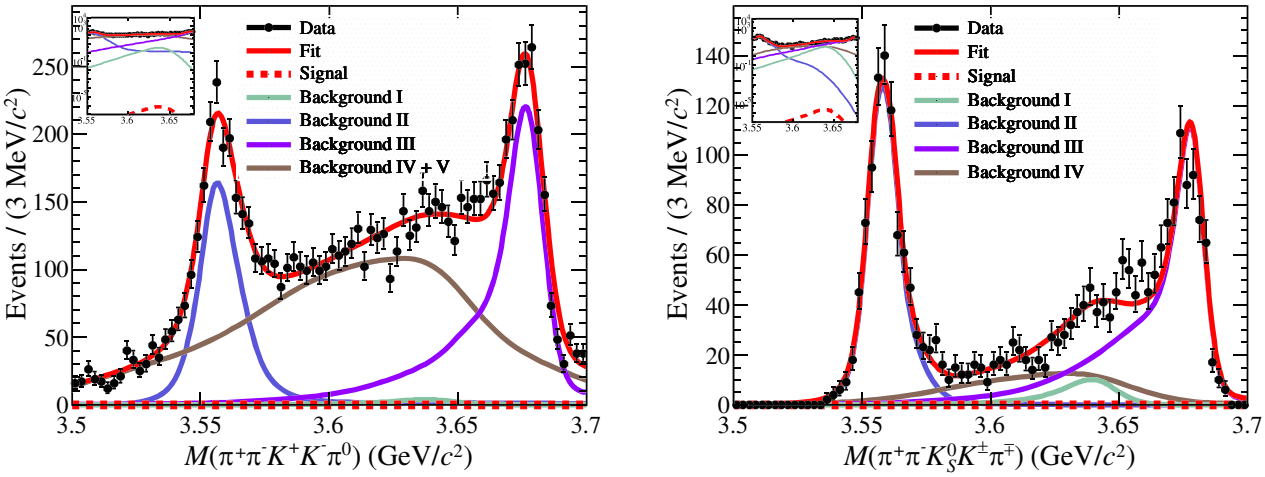

FIG. 3. The simultaneous fit to the distributions of (a) $M^{3C}(\pi^+\pi^-K^+K^-\pi^0)$ and (b) $M^{3C}(\pi^+\pi^-K^0_SK^\pm\pi^\mp)$, and the magnified view of the signal region on a logarithmic scale. The black dots with error bars are data, the red dotted lines are the signal, the green solid lines are the background I, the blue solid lines are the background II, the purple solid lines are the background III, the brown solid lines are other backgrounds IV + V in the left figure and IV in the right figure. The red solid lines are the total fit curves.

$\mathcal{B}(\psi(2S)\to\gamma\eta_c(2S))\times\mathcal{B}(\eta_c(2S)\to\pi^+\pi^-\eta_c)$ at the 90% CL is set using the Bayesian method [37]. First, we select the case that gives the largest upper limit after considering the additive systematic terms. Then, the obtained likelihood distribution as function of $\mathcal{B}(\psi(2S) \to \gamma\eta_c(2S)) \times \mathcal{B}(\eta_c(2S) \to \pi^+\pi^-\eta_c)$ is smeared with a Gaussian function with mean of 0 and width equal to the multiplicative systematic uncertainty [38]. Figure 4 shows the normalized likelihood distribution as a function of $\mathcal{B}(\psi(2S) \to \gamma\eta_c(2S)) \times \mathcal{B}(\eta_c(2S) \to \pi^+\pi^-\eta_c)$ after incorporating the systematic uncertainties. The upper limit on $\mathcal{B}(\psi(2S) \to \gamma\eta_c(2S)) \times \mathcal{B}(\eta_c(2S) \to \pi^+\pi^-\eta_c)$ is determined to be 2.21×10^{-5} at the 90% CL.

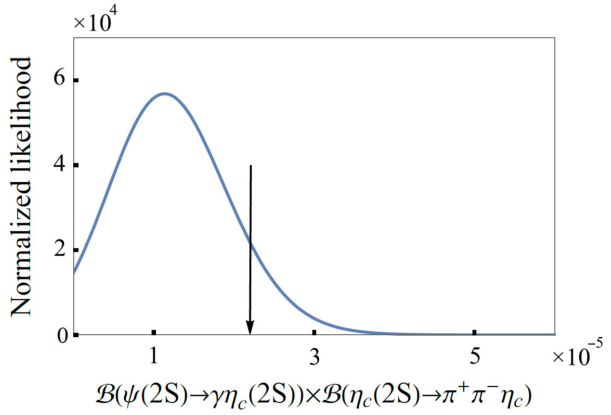

FIG. 4. Normalized likelihood versus $\mathcal{B}(\psi(2S) \to \gamma\eta_c(2S)) \times \mathcal{B}(\eta_c(2S) \to \pi^+\pi^-\eta_c)$ after incorporating the systematic uncertainties. The black arrow corresponds to the upper limit on the product branching fraction at the 90% CL.

IV. MEASUREMENT OF $\eta_c(2S) \to \pi^+\pi^-K^0_SK^\pm\pi^\mp$

A. Event selection

To investigate the $\eta_c(2S) \to \pi^+\pi^-K^0_SK^\pm\pi^\mp$ decay, we use almost the same selection criteria for $\psi(2S) \to \gamma\eta_c(2S)$, $\eta_c(2S) \to \pi^+\pi^-\eta_c$, $\eta_c \to K^0_SK^\pm\pi^\mp$, as described in Sec. III A, except for removing the η_c mass window. A 4C kinematic fit is performed under the $e^+e^- \to \gamma\pi^+\pi^-\pi^+\pi^-K^\pm\pi^\mp$ hypothesis, and χ^2_{4C} is required to be less than 25. Similarly, a 3C kinematic fit is performed and the four-momenta of daughter particles updated by the 3C kinematic fit are used for further analysis.

B. Background analysis

The analysis of the inclusive MC sample shows that the background events are mainly from $\psi(2S) \to \gamma\chi_{c1,2}$, $\chi_{c1,2} \to \pi^+\pi^-K^0_SK^\pm\pi^\mp$, $\psi(2S) \to (\gamma_{\rm FSR})\pi^+\pi^-K^0_SK^\pm\pi^\mp$, $\psi(2S) \to \pi^0\pi^+\pi^-K^0_SK^\pm\pi^\mp$, and other $\psi(2S)$ decays with pion or kaon misidentified.

The contribution of continuum production is estimated with the data sample at $\sqrt{s} = 3.650$ GeV. Its yield is normalized by a factor of 9.8 to account for the differences in the integrated luminosities and cross sections at $\sqrt{s} =$ 3.686 and 3.650 GeV. After normalization, the yield of the continuum production is fixed to be $N^{\rm con}_{\rm bkg} = 2812.6 \pm 53.0$.

C. Signal yield

The signal yield of $\eta_c(2S) \to \pi^+\pi^-K^0_SK^\pm\pi^\mp$ is extracted from an unbinned maximum likelihood fit to the $M(\pi^+\pi^-K^0_SK^\pm\pi^\mp)$ distribution. In the fit, the $\eta_c(2S)$ signal shape is described by Eq. (3) and the selected shapes and

TABLE II. The selected shapes and the yield types of different background sources for $\eta_c(2S) \to \pi^+\pi^- K^0_S K^\pm \pi^\mp$. All simulated shapes are derived from individual exclusive MC samples. '⊗ Gaussian' denotes that the simulated shapes are smeared with a Gaussian function with parameters obtained from the corresponding χ_{cJ} signal. To reduce the influence of statistical fluctuations, the shape of the continuum production has been smoothed via a fit with a Gaussian function and an ARGUS function.

No.	Source	Shape	Nature of yield
I	$\psi(2S) \to \gamma\chi_{c2}, \chi_{c2} \to \pi^+\pi^- K^0_S K^\pm \pi^\mp$	Simulated shape ⊗ Gaussian	Floated
II	$\psi(2S) \to \gamma\chi_{c1}, \chi_{c1} \to \pi^+\pi^- K^0_S K^\pm \pi^\mp$	Simulated shape	Floated
III	$\psi(2S) \to (\gamma_{\rm FSR})\pi^+\pi^- K^0_S K^\pm \pi^\mp$	Simulated shape ⊗ Gaussian	Floated
IV	Continuum production	Data @ 3.650 GeV	Fixed at $N^{\rm con}_{\rm bkg}$ (Sec. IV B)
V	$\psi(2S) \to \pi^0\pi^+\pi^- K^0_S K^\pm \pi^\mp$	Simulated shape	Floated
VI	$\psi(2S) \to \gamma\pi^+\pi^- K^0_S K^\pm \pi^\mp$	Simulated shape	Floated
VII	K/π misidentifications	Simulated shape	Floated

the nature of yields for different background components are summarized in Table II. Figure 5(a) shows the fit result and the relative pull distribution. The zoomed distribution of the fit result and the background-subtracted distribution in the $\eta_c(2S)$ signal region is shown in Fig. 5(b). From this fit, the signal yield of $\eta_c(2S) \to \pi^+\pi^- K^0_S K^\pm \pi^\mp$, $N'_{\rm sig}$, is obtained to be 3140 ± 241. The statistical significance of the signal is estimated to be 10σ from $\sqrt{-2\ln(\mathcal{L}_{\rm bkg}/\mathcal{L}_{\rm sig})}$ taking into account the difference in the number of degrees of freedom [39], where $\mathcal{L}_{\rm sig}$ and $\mathcal{L}_{\rm bkg}$ are the likelihoods with and without the signal, respectively, and the difference in the number of degrees of freedom is 1.

D. Branching fraction

The product branching fraction $\mathcal{B}(\psi(2S) \to \gamma\eta_c(2S)) \times \mathcal{B}(\eta_c(2S) \to \pi^+\pi^- K^0_S K^\pm \pi^\mp)$ is calculated as

$$\mathcal{B}_{\rm pro} = \frac{N'_{\rm sig}}{N_{\psi(2S)} \times \varepsilon'}, \tag{6}$$

where ε' is the detection efficiency estimated by MC simulation. The obtained results are shown in Table III. The product branching fraction $\mathcal{B}(\psi(2S) \to \gamma\eta_c(2S)) \times \mathcal{B}(\eta_c(2S) \to \pi^+\pi^- K^0_S K^\pm \pi^\mp)$ is determined to be $(9.31 \pm 0.72) \times 10^{-6}$. Taking the $\mathcal{B}(\psi(2S) \to \gamma\eta_c(2S)) = (7 \pm 5) \times 10^{-4}$ from the PDG [14] as input, the branching fraction of $\eta_c(2S) \to \pi^+\pi^- K^0_S K^\pm \pi^\mp$ is determined to be $(1.33 \pm 0.11) \times 10^{-2}$, where the uncertainty is statistical only.

V. SYSTEMATIC UNCERTAINTY

A. Systematic uncertainty for $\eta_c(2S) \to \pi^+\pi^-\eta_c$

The sources of systematic uncertainties are divided into two categories: additive and multiplicative terms.

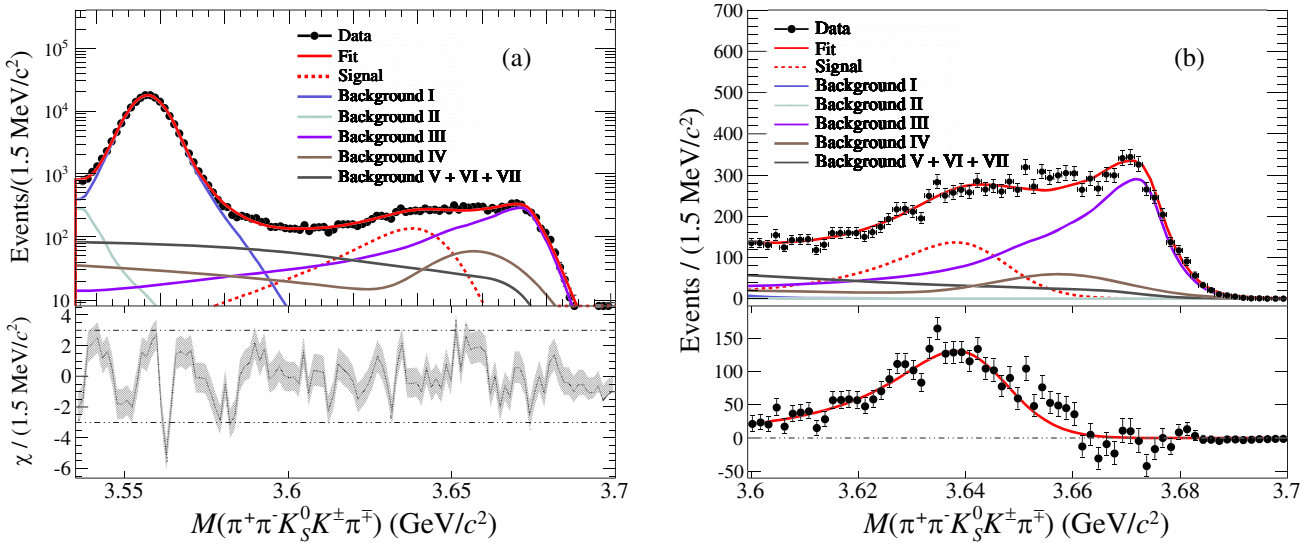

FIG. 5. (a) Fit to the distribution of $M^{\rm 3C}(\pi^+\pi^- K^0_S K^\pm \pi^\mp)$ and the relative pull distribution. (b) Zoomed $M^{\rm 3C}(\pi^+\pi^- K^0_S K^\pm \pi^\mp)$ distribution and background residuals. The black dots with error bars are data, the red dotted lines are the signal, the blue solid lines are the background I, the green solid lines are the background II, the purple solid lines are the background III, the brown solid lines are the background IV, the gray solid lines are for the remaining background V + VI + VII, and the red solid lines are the total fit curves.

TABLE III. The signal yields, signal efficiencies, and product branching fractions (upper limit at 90% CL) for $\psi(2S) \to \gamma\eta_c(2S)$ with $\eta_c(2S) \to \pi^+\pi^-\eta_c$ and $\eta_c(2S) \to \pi^+\pi^- K_S^0 K^\pm\pi^\mp$.

$\eta_c(2S)$ decay	η_c decay	$N_{\rm data}^{\rm sig}$	ε (%)	$\mathcal{B}_{\rm measured}$
$\eta_c(2S) \to \pi^+\pi^-\eta_c$	$\eta_c \to K^+K^-\pi^0$	⋯	11.4	$<2.21 \times 10^{-5}$
	$\eta_c \to K_S^0 K^\pm\pi^\mp$		12.0	
$\eta_c(2S) \to \pi^+\pi^- K_S^0 K^\pm\pi^\mp$	⋯	3140 ± 241	12.4	$(9.31 \pm 0.72 \pm 2.77) \times 10^{-6}$

The additive systematic uncertainties arise from the fit range, signal shape and background estimation. After considering all possible variations, the one that yields the largest upper limit is chosen as a conservative approach.

(i) The systematic uncertainty arising from the fit range is determined by changing the invariant mass fit range from $[3.5, 3.7]\ \mathrm{GeV}/c^2$ to $[3.52, 3.72]\ \mathrm{GeV}/c^2$ and $[3.51, 3.71]\ \mathrm{GeV}/c^2$.

(ii) The uncertainty associated with the η_c signal shape is estimated by changing the damping function from Eq. (4) to an alternative one used by the CLEO Collaboration [40], while $\eta_c(2S)$ mass is varied by $\pm 1\sigma$. The systematic uncertainty caused by the resolution difference between data and MC simulation for $\eta_c(2S) \to \pi^+\pi^-\eta_c$ is estimated by using the control samples of $\chi_{c2} \to \pi^+\pi^- K^+K^-\pi^0$ and $\chi_{c2} \to \pi^+\pi^- K_S^0 K^\pm\pi^\mp$. The obtained parameters of the smeared Gaussian function are used to replace those in the nominal one to describe the $\eta_c(2S)$ signal shape.

(iii) The systematic uncertainty due to the background shape is estimated by altering from the third-order to second-order Chebyshev polynomial function. The correction factor $f_{\rm corr}$ is changed by $\pm 1\sigma$ to evaluate the systematic uncertainty due to FSR. The uncertainty due to the peaking background is estimated by varying the fixed background yields by $\pm 1\sigma$.

The multiplicative systematic uncertainties apply to the determination of efficiency and branching fraction. These uncertainties include the following sources.

(i) The uncertainty of the total number of $\psi(2S)$ events in data is estimated to be 0.5% [41].

(ii) The systematic uncertainty due to the tracking efficiency for charged tracks is determined to be 1.0% per track using the control samples of $J/\psi \to \pi^0\pi^+\pi^-, J/\psi \to p\bar{p}\pi^+\pi^-$ and $J/\psi \to K_S^0 K^\pm\pi^\mp$ + c.c. [42].

(iii) The systematic uncertainty due to the photon detection efficiency is 1.0% per photon, which is determined from the control samples of $J/\psi \to \rho^0\pi^0$ and $e^+e^- \to \gamma\gamma$ [43].

(iv) The systematic uncertainty due to the K_S^0 reconstruction is studied using control samples of $J/\psi \to K^{*\pm}K^\mp$ and $J/\psi \to \phi K_S^0 K^\pm\pi^\mp$, and estimated to be 1.0%.

(v) Using a high purity control sample of $J/\psi \to \pi^0\bar{p}p$, the systematic uncertainty from the π^0 reconstruction is assigned to be 1.0% [44].

(vi) The systematic uncertainty associated with the kinematic fit is assigned as the difference between the detection efficiencies before and after the helix parameter corrections [45] in the MC simulation, which are 2.0% for $\eta_c(2S) \to \pi^+\pi^-\eta_c$, $\eta_c \to K_S^0 K^\pm\pi^\mp$, and 2.5% for $\eta_c(2S) \to \pi^+\pi^-\eta_c$, $\eta_c \to K^+K^-\pi^0$.

(vii) To evaluate the systematic uncertainty due to the J/ψ veto, we vary the requirement on the recoil mass of $\pi^+\pi^-$ by $\pm 10\ \mathrm{MeV}/c^2$. The maximum deviation in the measured branching fraction is taken as the systematic uncertainty.

(viii) The systematic uncertainty arising from the η_c mass window is estimated by adjusting the mass window by $\pm 10\ \mathrm{MeV}/c^2$. The maximum difference in the branching fraction with respect to the nominal value is taken as the systematic uncertainty.

(ix) To evaluate the systematic uncertainty due to the ω veto, we change the mass window of ω by $\pm 1\ \mathrm{MeV}/c^2$. The maximum deviation in the measured branching fraction is taken as the systematic uncertainty.

(x) The uncertainties from the branching fractions of $\psi(2S) \to \gamma\eta_c(2S)$, $\eta_c \to K^+K^-\pi^0$ and $\eta_c \to K_S^0 K^\pm\pi^\mp$ quoted from the PDG are 71.4% [14], 13.6% and 11.2% [33], respectively.

Table IV summarizes the multiplicative systematic uncertainties. The combined relative systematic uncertainty is calculated by [46]

$$\sigma_{\rm sum}^i = \frac{\sqrt{(\omega_1\delta_1^i)^2 + (\omega_2\delta_2^i)^2 + 2\omega_1\omega_2\rho_{12}^i\delta_1^i\delta_2^i}}{\omega_1 + \omega_2}, \quad (7)$$

where ω_1 and ω_2 are $\mathcal{B}(\eta_c \to K^+K^-\pi^0) \times \varepsilon_3$ and $\mathcal{B}(\eta_c \to K_S^0 K^\pm\pi^\mp) \times \varepsilon_4$, δ_1^i and δ_2^i are the corresponding multiplicative uncertainties for $\eta_c(2S) \to \pi^+\pi^-\eta_c, \eta_c \to K^+K^-\pi^0$ and $\eta_c \to K_S^0 K^\pm\pi^\mp$, respectively. The correlation coefficiency ρ_{12} is taken as 0 for those items that are uncorrelated between the two decay modes of $\eta_c(2S) \to \pi^+\pi^-\eta_c, \eta_c \to K^+K^-\pi^0$ and $\eta_c \to K_S^0 K^\pm\pi^\mp$, including η_c mass window, K_S^0 reconstruction, J/ψ veto, ω veto, and branching faction of η_c decay. For other systematic effects

TABLE IV. Multiplicative systematic uncertainties (in %) in the measured branching fraction for $\eta_c(2S) \to \pi^+\pi^-\eta_c$.

Source	$\eta_c(2S)\to\pi^+\pi^-\eta_c$, $\eta_c\to K^0_S K^\pm\pi^\mp$	$\eta_c(2S)\to\pi^+\pi^-\eta_c$, $\eta_c\to K^+K^-\pi^0$	$\sigma^i_{\rm sum}$
$N_{\psi(2S)}$	0.5	0.5	0.5
Tracking	6.0	4.0	5.4
Photon reconstruction	1.0	3.0	1.6
K^0_S reconstruction	1.0	...	0.7
π^0 reconstruction	...	1.0	0.3
Kinematic fit	2.0	2.5	2.1
J/ψ veto	4.4	4.0	3.3
η_c mass window	4.0	4.0	3.1
ω veto	...	0.1	0.03
η_c decay	11.2	13.6	8.9
Total	14.2	15.8	11.7
$\mathcal{B}(\psi(2S)\to\gamma\eta_c(2S))$	71.4		

that are correlated between these two decay modes, ρ_{12} is taken as 1. Finally, the total combined systematic uncertainty $\sigma_{\rm sum}$ is assigned as

$$\sigma_{\rm sum} = \sqrt{\Sigma(\sigma^i_{\rm sum})^2}, \tag{8}$$

which is listed in the last column in Table IV.

B. Systematic uncertainty for $\eta_c(2S) \to \pi^+\pi^- K^0_S K^\pm\pi^\mp$

The systematic uncertainties in the measurement of the branching fraction of $\eta_c(2S) \to \pi^+\pi^- K^0_S K^\pm\pi^\mp$ are summarized in Table V.

The systematic uncertainties due to the tracking efficiency, photon reconstruction, K^0_S reconstruction, total number of $\psi(2S)$ events, kinematic fit, J/ψ veto, fit range, and signal shape are estimated with the same methods introduced in Sec. V A.

The systematic uncertainties due to the background estimation are estimated by changing the correction factor $f_{\rm corr}$ by $\pm1\sigma$, changing the parametrization of continuum background, and changing the model of the cross-section dependence on the center-of-mass energy.

TABLE V. Relative systematic uncertainties (%) in the measurement of the product branching fraction $\mathcal{B}(\psi(2S) \to \gamma\eta_c(2S)) \times \mathcal{B}(\eta_c(2S) \to \pi^+\pi^- K^0_S K^\pm\pi^\mp)$.

Source	Uncertainty
$N_{\psi(2S)}$	0.5
Tracking	6.0
Photon reconstruction	1.0
K^0_S reconstruction	1.0
Kinematic fit	2.0
J/ψ veto	3.8
Fit range	3.8
Signal shape	18.9
Background estimation	21.5
Total	29.8

VI. SUMMARY

Based on $(27.12 \pm 0.14) \times 10^8$ $\psi(2S)$ events collected by the BESIII detector, we search for $\eta_c(2S) \to \pi^+\pi^-\eta_c$ with $\eta_c \to K^0_S K^\pm\pi^\mp$ and $\eta_c \to K^+K^-\pi^0$. No significant signal of $\eta_c(2S) \to \pi^+\pi^-\eta_c$ is observed, and the upper limit on the product branching fraction $\mathcal{B}(\psi(2S) \to \gamma\eta_c(2S)) \times \mathcal{B}(\eta_c(2S) \to \pi^+\pi^-\eta_c)$ is determined to be 2.21×10^{-5} at the 90% CL. In addition, we present the first observation of $\eta_c(2S) \to \pi^+\pi^- K^0_S K^\pm\pi^\mp$ with a statistical significance of 10σ. The branching fraction of $\eta_c(2S) \to \pi^+\pi^- K^0_S K^\pm\pi^\mp$ is measured to be $(1.33 \pm 0.11 \pm 0.4 \pm 0.95)\times10^{-2}$, where the first and second uncertainties are statistical and systematic, respectively, and the third uncertainty is from the quoted branching fraction of $\psi(2S) \to \gamma\eta_c(2S)$ [14]. The obtained result is consistent with our previous measurement [17], but with improved precision.

ACKNOWLEDGMENTS

The BESIII Collaboration thanks the staff of BEPCII and the IHEP computing center for their strong support. This work is supported in part by National Key R&D Program of China under Contracts No. 2023YFA1606704, No. 2020YFA0406300, No. 2020YFA0406400; National Natural Science Foundation of China (NSFC) under Contracts No. 12275058, No. 11635010, No. 11735014, No. 11835012, No. 11935015, No. 11935016, No. 11935018, No. 11961141012, No. 12025502, No. 12035009, No. 12035013, No. 12061131003, No. 12192260, No. 12192261, No. 12192262, No. 12192263, No. 12192264, No. 12192265,

No. 12221005, No. 12225509, No. 12235017; the Chinese Academy of Sciences (CAS) Large-Scale Scientific Facility Program; the CAS Center for Excellence in Particle Physics (CCEPP); Joint Large-Scale Scientific Facility Funds of the NSFC and CAS under Contract No. U1832207; CAS Key Research Program of Frontier Sciences under Contracts No. QYZDJ-SSW-SLH003, No. QYZDJ-SSW-SLH040; 100 Talents Program of CAS; The Institute of Nuclear and Particle Physics (INPAC) and Shanghai Key Laboratory for Particle Physics and Cosmology; European Union's Horizon 2020 research and innovation programme under Marie Sklodowska-Curie grant agreement under Contract No. 894790; German Research Foundation DFG under Contracts Nos. 455635585, Collaborative Research Center CRC 1044, FOR5327, GRK 2149; Istituto Nazionale di Fisica Nucleare, Italy; Ministry of Development of Turkey under Contract No. DPT2006K-120470; National Research Foundation of Korea under Contract No. NRF-2022R1A2C1092335; National Science and Technology fund of Mongolia; National Science Research and Innovation Fund (NSRF) via the Program Management Unit for Human Resources & Institutional Development, Research and Innovation of Thailand under Contract No. B16F640076; Polish National Science Centre under Contract No. 2019/35/O/ST2/02907; The Swedish Research Council; U.S. Department of Energy under Contract No. DE-FG02-05ER41374.

[1] N. Brambilla, M. Á. Escobedo, J. Ghiglieri, and A. Vairo, J. High Energy Phys. 07 (**2011**) 096.
[2] S. K. Choi *et al.* (Belle Collaboration), Phys. Rev. Lett. **89**, 102001 (2002); **89**, 129901(E) (2002).
[3] B. Aubert *et al.* (*BABAR* Collaboration), Phys. Rev. Lett. **92**, 142002 (2004).
[4] K. K. Seth (CLEO Collaboration), AIP Conf. Proc. **717**, 543 (2004).
[5] H. Nakazawa *et al.* (Belle Collaboration), Nucl. Phys. B, Proc. Suppl. **184**, 220 (2008).
[6] B. Aubert *et al.* (*BABAR* Collaboration), Phys. Rev. D **72**, 031101 (2005).
[7] K. Abe *et al.* (Belle Collaboration), Phys. Rev. Lett. **98**, 082001 (2007).
[8] M. Ablikim *et al.* (BESIII Collaboration), Phys. Rev. Lett. **109**, 042003 (2012).
[9] G. S. Abrams *et al.*, Phys. Rev. Lett. **34**, 1181 (1975).
[10] M. B. Voloshin, JETP Lett. **21**, 347 (1975).
[11] L. S. Brown, and R. N. Cahn, Phys. Rev. Lett. **35**, 1 (1975).
[12] M. B. Voloshin, Mod. Phys. Lett. A **17**, 1533 (2002).
[13] J. Z. Bai *et al.* (BES Collaboration), Phys. Rev. D **62**, 032002 (2000).
[14] R. L. Workman *et al.* (Particle Data Group), Prog. Theor. Exp. Phys. **2022**, 083C01 (2022).
[15] M. B. Voloshin, Phys. Rev. D **74**, 054022 (2006).
[16] J. P. Lees *et al.* (*BABAR* Collaboration), Phys. Rev. D **86**, 092005 (2012).
[17] M. Ablikim *et al.* (BESIII Collaboration), Phys. Rev. D **87**, 052005 (2013).
[18] M. Ablikim *et al.* (BESIII Collaboration), Nucl. Instrum. Methods Phys. Res., Sect. A **614**, 345 (2010).
[19] F. A. Harris, Int. J. Mod. Phys. A **24**, 0904370 (2008).
[20] M. Ablikim *et al.* (BESIII Collaboration), Chin. Phys. C **44**, 040001 (2020).
[21] J.-W. Zhang *et al.*, Radiat. Detect. Technol. Methods **6**, 289 (2022).
[22] X. Li *et al.*, Radiat. Detect. Technol. Methods **1**, 13 (2017).
[23] Y.-X. Guo *et al.*, Radiat. Detect. Technol. Methods **1**, 15 (2017).
[24] P. Cao *et al.*, Nucl. Instrum. Methods Phys. Res., Sect. A **953**, 163053 (2020).
[25] S. Agostinelli *et al.* (GEANT4 Collaboration), Nucl. Instrum. Methods Phys. Res., Sect. A **506**, 250 (2003).
[26] S. Jadach, B. F. L. Ward, and Z. Was, Comput. Phys. Commun. **130**, 260 (2000).
[27] S. Jadach, B. F. L. Ward, and Z. Was, Phys. Rev. D **63**, 113009 (2001).
[28] D. J. Lange, Nucl. Instrum. Methods Phys. Res., Sect. A **462**, 152 (2001).
[29] R.-G. Ping, Chin. Phys. C **32**, 599 (2008).
[30] J. C. Chen, G. S. Huang, X. R. Qi, D. H. Zhang, and Y. S. Zhu, Phys. Rev. D **62**, 034003 (2000).
[31] R.-L. Yang, R.-G. Ping, and H. Chen, Chin. Phys. Lett. **31**, 061301 (2014).
[32] W. M. Tanenbaum *et al.*, Phys. Rev. D **17**, 1731 (1978).
[33] M. Ablikim *et al.* (BESIII Collaboration), Phys. Rev. D **86**, 092009 (2012).
[34] S. Bityukov, arXiv:physics/9809037.
[35] M. Ablikim *et al.* (BESIII Collaboration), Phys. Rev. D **106**, 032014 (2022).
[36] V. V. Anashin *et al.*, Chin. Phys. C **34**, 831 (2010).
[37] J. Conrad, O. Botner, A. Hallgren, and C. Pérez de los Heros, Phys. Rev. D **67**, 012002 (2003).
[38] K. Stenson, arXiv:physics/0605236.
[39] S. S. Wilks, Ann. Math. Stat. **9**, 60 (1938).
[40] R. E. Mitchell (CLEO Collaboration), Phys. Rev. Lett. **102**, 011801 (2008).
[41] M. Ablikim *et al.* (BESIII Collaboration), Chin. Phys. C **42**, 023001 (2018).
[42] M. Ablikim *et al.* (BESIII Collaboration), Phys. Rev. D **83**, 112005 (2011).

[43] M. Ablikim *et al.* (BESIII Collaboration), Phys. Rev. D **81**, 052005 (2010).
[44] M. Ablikim *et al.* (BESIII Collaboration), Phys. Rev. Lett. **105**, 261801 (2010).
[45] M. Ablikim *et al.* (BESIII Collaboration), Phys. Rev. D **87**, 012002 (2013).
[46] M. Ablikim *et al.* (BESIII Collaboration), Phys. Rev. D **107**, 072003 (2023).

M. Ablikim,[1] M. N. Achasov,[4,c] P. Adlarson,[75] O. Afedulidis,[3] X. C. Ai,[80] R. Aliberti,[35] A. Amoroso,[74a,74c] Q. An,[71,58,a] Y. Bai,[57] O. Bakina,[36] I. Balossino,[29a] Y. Ban,[46,h] H.-R. Bao,[63] V. Batozskaya,[1,44] K. Begzsuren,[32] N. Berger,[35] M. Berlowski,[44] M. Bertani,[28a] D. Bettoni,[29a] F. Bianchi,[74a,74c] E. Bianco,[74a,74c] A. Bortone,[74a,74c] I. Boyko,[36] R. A. Briere,[5] A. Brueggemann,[68] H. Cai,[76] X. Cai,[1,58] A. Calcaterra,[28a] G. F. Cao,[1,63] N. Cao,[1,63] S. A. Cetin,[62a] J. F. Chang,[1,58] G. R. Che,[43] G. Chelkov,[36,b] C. Chen,[43] C. H. Chen,[9] Chao Chen,[55] G. Chen,[1] H. S. Chen,[1,63] H. Y. Chen,[20] M. L. Chen,[1,58,63] S. J. Chen,[42] S. L. Chen,[45] S. M. Chen,[61] T. Chen,[1,63] X. R. Chen,[31,63] X. T. Chen,[1,63] Y. B. Chen,[1,58] Y. Q. Chen,[34] Z. J. Chen,[25,i] Z. Y. Chen,[1,63] S. K. Choi,[10] G. Cibinetto,[29a] F. Cossio,[74c] J. J. Cui,[50] H. L. Dai,[1,58] J. P. Dai,[78] A. Dbeyssi,[18] R. E. de Boer,[3] D. Dedovich,[36] C. Q. Deng,[72] Z. Y. Deng,[1] A. Denig,[35] I. Denysenko,[36] M. Destefanis,[74a,74c] F. De Mori,[74a,74c] B. Ding,[66,1] X. X. Ding,[46,h] Y. Ding,[34] Y. Ding,[40] J. Dong,[1,58] L. Y. Dong,[1,63] M. Y. Dong,[1,58,63] X. Dong,[76] M. C. Du,[1] S. X. Du,[80] Y. Y. Duan,[55] Z. H. Duan,[42] P. Egorov,[36,b] Y. H. Fan,[45] J. Fang,[59] J. Fang,[1,58] S. S. Fang,[1,63] W. X. Fang,[1] Y. Fang,[1] Y. Q. Fang,[1,58] R. Farinelli,[29a] L. Fava,[74b,74c] F. Feldbauer,[3] G. Felici,[28a] C. Q. Feng,[71,58] J. H. Feng,[59] Y. T. Feng,[71,58] M. Fritsch,[3] C. D. Fu,[1] J. L. Fu,[63] Y. W. Fu,[1,63] H. Gao,[63] X. B. Gao,[41] Y. N. Gao,[46,h] Yang Gao,[71,58] S. Garbolino,[74c] I. Garzia,[29a,29b] L. Ge,[80] P. T. Ge,[76] Z. W. Ge,[42] C. Geng,[59] E. M. Gersabeck,[67] A. Gilman,[69] K. Goetzen,[13] L. Gong,[40] W. X. Gong,[1,58] W. Gradl,[35] S. Gramigna,[29a,29b] M. Greco,[74a,74c] M. H. Gu,[1,58] Y. T. Gu,[15] C. Y. Guan,[1,63] Z. L. Guan,[22] A. Q. Guo,[31,63] L. B. Guo,[41] M. J. Guo,[50] R. P. Guo,[49] Y. P. Guo,[12,g] A. Guskov,[36,b] J. Gutierrez,[27] K. L. Han,[63] T. T. Han,[1] F. Hanisch,[3] X. Q. Hao,[19] F. A. Harris,[65] K. K. He,[55] K. L. He,[1,63] F. H. Heinsius,[3] C. H. Heinz,[35] Y. K. Heng,[1,58,63] C. Herold,[60] T. Holtmann,[3] P. C. Hong,[34] G. Y. Hou,[1,63] X. T. Hou,[1,63] Y. R. Hou,[63] Z. L. Hou,[1] B. Y. Hu,[59] H. M. Hu,[1,63] J. F. Hu,[56,j] S. L. Hu,[12,g] T. Hu,[1,58,63] Y. Hu,[1] G. S. Huang,[71,58] K. X. Huang,[59] L. Q. Huang,[31,63] X. T. Huang,[50] Y. P. Huang,[1] T. Hussain,[73] F. Hölzken,[3] N. Hüsken,[27,35] N. Hüsken,[35] N. in der Wiesche,[68] J. Jackson,[27] S. Janchiv,[32] J. H. Jeong,[10] Q. Ji,[1] Q. P. Ji,[19] W. Ji,[1,63] X. B. Ji,[1,63] X. L. Ji,[1,58] Y. Y. Ji,[50] X. Q. Jia,[50] Z. K. Jia,[71,58] D. Jiang,[1,63] H. B. Jiang,[76] P. C. Jiang,[46,h] S. S. Jiang,[39] T. J. Jiang,[16] X. S. Jiang,[1,58,63] Y. Jiang,[63] J. B. Jiao,[50] J. K. Jiao,[34] Z. Jiao,[23] S. Jin,[42] Y. Jin,[66] M. Q. Jing,[1,63] X. M. Jing,[63] T. Johansson,[75] S. Kabana,[33] N. Kalantar-Nayestanaki,[64] X. L. Kang,[9] X. S. Kang,[40] M. Kavatsyuk,[64] B. C. Ke,[80] V. Khachatryan,[27] A. Khoukaz,[68] R. Kiuchi,[1] O. B. Kolcu,[62a] B. Kopf,[3] M. Kuessner,[3] X. Kui,[1,63] N. Kumar,[26] A. Kupsc,[44,75] W. Kühn,[37] J. J. Lane,[67] P. Larin,[18] L. Lavezzi,[74a,74c] T. T. Lei,[71,58] Z. H. Lei,[71,58] M. Lellmann,[35] T. Lenz,[35] C. Li,[47] C. Li,[43] C. H. Li,[39] Cheng Li,[71,58] D. M. Li,[80] F. Li,[1,58] G. Li,[1] H. B. Li,[1,63] H. J. Li,[19] H. N. Li,[56,j] Hui Li,[43] J. R. Li,[61] J. S. Li,[59] Ke Li,[1] L. J. Li,[1,63] L. K. Li,[1] Lei Li,[48] M. H. Li,[43] P. R. Li,[38,l] Q. M. Li,[1,63] Q. X. Li,[50] R. Li,[17,31] S. X. Li,[12] T. Li,[50] W. D. Li,[1,63] W. G. Li,[1,a] X. Li,[1,63] X. H. Li,[71,58] X. L. Li,[50] X. Z. Li,[59] Xiaoyu Li,[1,63] Y. G. Li,[46,h] Z. J. Li,[59] Z. X. Li,[15] Z. Y. Li,[78] C. Liang,[42] H. Liang,[71,58] H. Liang,[1,63] Y. F. Liang,[54] Y. T. Liang,[31,63] G. R. Liao,[14] L. Z. Liao,[50] J. Libby,[26] A. Limphirat,[60] C. C. Lin,[55] D. X. Lin,[31,63] T. Lin,[1] B. J. Liu,[1] B. X. Liu,[76] C. Liu,[34] C. X. Liu,[1] F. H. Liu,[53] Fang Liu,[1] Feng Liu,[6] G. M. Liu,[56,j] H. Liu,[38,k,l] H. B. Liu,[15] H. M. Liu,[1,63] Huanhuan Liu,[1] Huihui Liu,[21] J. B. Liu,[71,58] J. Y. Liu,[1,63] K. Liu,[38,k,l] K. Y. Liu,[40] Ke Liu,[22] L. Liu,[71,58] L. C. Liu,[43] Lu Liu,[43] M. H. Liu,[12,g] P. L. Liu,[1] Q. Liu,[63] S. B. Liu,[71,58] T. Liu,[12,g] W. K. Liu,[43] W. M. Liu,[71,58] X. Liu,[39] X. Liu,[38,k,l] Y. Liu,[38,k,l] Y. Liu,[80] Y. B. Liu,[43] Z. A. Liu,[1,58,63] Z. D. Liu,[9] Z. Q. Liu,[50] X. C. Lou,[1,58,63] F. X. Lu,[59] H. J. Lu,[23] J. G. Lu,[1,58] X. L. Lu,[1] Y. Lu,[7] Y. P. Lu,[1,58] Z. H. Lu,[1,63] C. L. Luo,[41] M. X. Luo,[79] T. Luo,[12,g] X. L. Luo,[1,58] X. R. Lyu,[63] Y. F. Lyu,[43] F. C. Ma,[40] H. Ma,[78] H. L. Ma,[1] J. L. Ma,[1,63] L. L. Ma,[50] M. M. Ma,[1,63] Q. M. Ma,[1] R. Q. Ma,[1,63] T. Ma,[71,58] X. T. Ma,[1,63] X. Y. Ma,[1,58] Y. Ma,[46,h] Y. M. Ma,[31] F. E. Maas,[18] M. Maggiora,[74a,74c] S. Malde,[69] Y. J. Mao,[46,h] Z. P. Mao,[1] S. Marcello,[74a,74c] Z. X. Meng,[66] J. G. Messchendorp,[13,64] G. Mezzadri,[29a] H. Miao,[1,63] T. J. Min,[42] R. E. Mitchell,[27] X. H. Mo,[1,58,63] B. Moses,[27] N. Yu. Muchnoi,[4,c] J. Muskalla,[35] Y. Nefedov,[36] F. Nerling,[18,e] L. S. Nie,[20] I. B. Nikolaev,[4,c] Z. Ning,[1,58] S. Nisar,[11,m] Q. L. Niu,[38,k,l] W. D. Niu,[55] Y. Niu,[50] S. L. Olsen,[63] Q. Ouyang,[1,58,63] S. Pacetti,[28b,28c] X. Pan,[55] Y. Pan,[57] A. Pathak,[34] P. Patteri,[28a] Y. P. Pei,[71,58] M. Pelizaeus,[3] H. P. Peng,[71,58] Y. Y. Peng,[38,k,l] K. Peters,[13,e] J. L. Ping,[41] R. G. Ping,[1,63] S. Plura,[35] V. Prasad,[33] F. Z. Qi,[1] H. Qi,[71,58] H. R. Qi,[61] M. Qi,[42] T. Y. Qi,[12,g] S. Qian,[1,58] W. B. Qian,[63] C. F. Qiao,[63] X. K. Qiao,[80] J. J. Qin,[72] L. Q. Qin,[14] L. Y. Qin,[71,58] X. S. Qin,[50] Z. H. Qin,[1,58] J. F. Qiu,[1] Z. H. Qu,[72]

C. F. Redmer,[35] K. J. Ren,[39] A. Rivetti,[74c] M. Rolo,[74c] G. Rong,[1,63] Ch. Rosner,[18] S. N. Ruan,[43] N. Salone,[44] A. Sarantsev,[36,d] Y. Schelhaas,[35] K. Schoenning,[75] M. Scodeggio,[29a] K. Y. Shan,[12,g] W. Shan,[24] X. Y. Shan,[71,58] Z. J. Shang,[38,k,l] J. F. Shangguan,[55] L. G. Shao,[1,63] M. Shao,[71,58] C. P. Shen,[12,g] H. F. Shen,[1,8] W. H. Shen,[63] X. Y. Shen,[1,63] B. A. Shi,[63] H. Shi,[71,58] H. C. Shi,[71,58] J. L. Shi,[12,g] J. Y. Shi,[1] Q. Q. Shi,[55] S. Y. Shi,[72] X. Shi,[1,58] J. J. Song,[19] T. Z. Song,[59] W. M. Song,[34,1] Y. J. Song,[12,g] Y. X. Song,[46,h,n] S. Sosio,[74a,74c] S. Spataro,[74a,74c] F. Stieler,[35] Y. J. Su,[63] G. B. Sun,[76] G. X. Sun,[1] H. Sun,[63] H. K. Sun,[1] J. F. Sun,[19] K. Sun,[61] L. Sun,[76] S. S. Sun,[1,63] T. Sun,[51,f] W. Y. Sun,[34] Y. Sun,[9] Y. J. Sun,[71,58] Y. Z. Sun,[1] Z. Q. Sun,[1,63] Z. T. Sun,[50] C. J. Tang,[54] G. Y. Tang,[1] J. Tang,[59] M. Tang,[71,58] Y. A. Tang,[76] L. Y. Tao,[72] Q. T. Tao,[25,i] M. Tat,[69] J. X. Teng,[71,58] V. Thoren,[75] W. H. Tian,[59] Y. Tian,[31,63] Z. F. Tian,[76] I. Uman,[62b] Y. Wan,[55] S. J. Wang,[50] B. Wang,[1] B. L. Wang,[63] Bo Wang,[71,58] D. Y. Wang,[46,h] F. Wang,[72] H. J. Wang,[38,k,l] J. J. Wang,[76] J. P. Wang,[50] K. Wang,[1,58] L. L. Wang,[1] M. Wang,[50] Meng Wang,[1,63] N. Y. Wang,[63] S. Wang,[38,k,l] S. Wang,[12,g] T. Wang,[12,g] T. J. Wang,[43] W. Wang,[72] W. Wang,[59] W. P. Wang,[35,71,o] X. Wang,[46,h] X. F. Wang,[38,k,l] X. J. Wang,[39] X. L. Wang,[12,g] X. N. Wang,[1] Y. Wang,[61] Y. D. Wang,[45] Y. F. Wang,[1,58,63] Y. L. Wang,[19] Y. N. Wang,[45] Y. Q. Wang,[1] Yaqian Wang,[17] Yi Wang,[61] Z. Wang,[1,58] Z. L. Wang,[72] Z. Y. Wang,[1,63] Ziyi Wang,[63] D. H. Wei,[14] F. Weidner,[68] S. P. Wen,[1] Y. R. Wen,[39] U. Wiedner,[3] G. Wilkinson,[69] M. Wolke,[75] L. Wollenberg,[3] C. Wu,[39] J. F. Wu,[1,8] L. H. Wu,[1] L. J. Wu,[1,63] X. Wu,[12,g] X. H. Wu,[34] Y. Wu,[71,58] Y. H. Wu,[55] Y. J. Wu,[31] Z. Wu,[1,58] L. Xia,[71,58] X. M. Xian,[39] B. H. Xiang,[1,63] T. Xiang,[46,h] D. Xiao,[38,k,l] G. Y. Xiao,[42] S. Y. Xiao,[1] Y. L. Xiao,[12,g] Z. J. Xiao,[41] C. Xie,[42] X. H. Xie,[46,h] Y. Xie,[50] Y. G. Xie,[1,58] Y. H. Xie,[6] Z. P. Xie,[71,58] T. Y. Xing,[1,63] C. F. Xu,[1,63] C. J. Xu,[59] G. F. Xu,[1] H. Y. Xu,[66] M. Xu,[71,58] Q. J. Xu,[16] Q. N. Xu,[30] W. Xu,[1] W. L. Xu,[66] X. P. Xu,[55] Y. C. Xu,[77] Z. P. Xu,[42] Z. S. Xu,[63] F. Yan,[12,g] L. Yan,[12,g] W. B. Yan,[71,58] W. C. Yan,[80] X. Q. Yan,[1] H. J. Yang,[51,f] H. L. Yang,[34] H. X. Yang,[1] Tao Yang,[1] Y. Yang,[12,g] Y. F. Yang,[43] Y. X. Yang,[1,63] Yifan Yang,[1,63] Z. W. Yang,[38,k,l] Z. P. Yao,[50] M. Ye,[1,58] M. H. Ye,[8] J. H. Yin,[1] Z. Y. You,[59] B. X. Yu,[1,58,63] C. X. Yu,[43] G. Yu,[1,63] J. S. Yu,[25,i] T. Yu,[72] X. D. Yu,[46,h] Y. C. Yu,[80] C. Z. Yuan,[1,63] J. Yuan,[34] L. Yuan,[2] S. C. Yuan,[1] Y. Yuan,[1,63] Y. J. Yuan,[45] Z. Y. Yuan,[59] C. X. Yue,[39] A. A. Zafar,[73] F. R. Zeng,[50] S. H. Zeng,[72] X. Zeng,[12,g] Y. Zeng,[25,i] Y. J. Zeng,[59] X. Y. Zhai,[34] Y. C. Zhai,[50] Y. H. Zhan,[59] A. Q. Zhang,[1,63] B. L. Zhang,[1,63] B. X. Zhang,[1] D. H. Zhang,[43] G. Y. Zhang,[19] H. Zhang,[80] H. Zhang,[71,58] H. C. Zhang,[1,58,63] H. H. Zhang,[59] H. H. Zhang,[34] H. Q. Zhang,[1,58,63] H. R. Zhang,[71,58] H. Y. Zhang,[1,58] J. Zhang,[80] J. Zhang,[59] J. J. Zhang,[52] J. L. Zhang,[20] J. Q. Zhang,[41] J. S. Zhang,[12,g] J. W. Zhang,[1,58,63] J. X. Zhang,[38,k,l] J. Y. Zhang,[1] J. Z. Zhang,[1,63] Jianyu Zhang,[63] L. M. Zhang,[61] Lei Zhang,[42] P. Zhang,[1,63] Q. Y. Zhang,[34] R. Y. Zhang,[38,k,l] Shuihan Zhang,[1,63] Shulei Zhang,[25,i] X. D. Zhang,[45] X. M. Zhang,[1] X. Y. Zhang,[50] Y. Zhang,[72] Y. T. Zhang,[80] Y. H. Zhang,[1,58] Y. M. Zhang,[39] Yan Zhang,[71,58] Yao Zhang,[1] Z. D. Zhang,[1] Z. H. Zhang,[1] Z. L. Zhang,[34] Z. Y. Zhang,[76] Z. Y. Zhang,[43] Z. Z. Zhang,[45] G. Zhao,[1] J. Y. Zhao,[1,63] J. Z. Zhao,[1,58] Lei Zhao,[71,58] Ling Zhao,[1] M. G. Zhao,[43] N. Zhao,[78] R. P. Zhao,[63] S. J. Zhao,[80] Y. B. Zhao,[1,58] Y. X. Zhao,[31,63] Z. G. Zhao,[71,58] A. Zhemchugov,[36,b] B. Zheng,[72] B. M. Zheng,[34] J. P. Zheng,[1,58] W. J. Zheng,[1,63] Y. H. Zheng,[63] B. Zhong,[41] X. Zhong,[59] H. Zhou,[50] J. Y. Zhou,[34] L. P. Zhou,[1,63] S. Zhou,[6] X. Zhou,[76] X. K. Zhou,[6] X. R. Zhou,[71,58] X. Y. Zhou,[39] Y. Z. Zhou,[12,g] J. Zhu,[43] K. Zhu,[1] K. J. Zhu,[1,58,63] K. S. Zhu,[12,g] L. Zhu,[34] L. X. Zhu,[63] S. H. Zhu,[70] S. Q. Zhu,[42] T. J. Zhu,[12,g] W. D. Zhu,[41] Y. C. Zhu,[71,58] Z. A. Zhu,[1,63] J. H. Zou,[1] and J. Zu[71,58]

(BESIII Collaboration)

[1]*Institute of High Energy Physics, Beijing 100049, People's Republic of China*
[2]*Beihang University, Beijing 100191, People's Republic of China*
[3]*Bochum Ruhr-University, D-44780 Bochum, Germany*
[4]*Budker Institute of Nuclear Physics SB RAS (BINP), Novosibirsk 630090, Russia*
[5]*Carnegie Mellon University, Pittsburgh, Pennsylvania 15213, USA*
[6]*Central China Normal University, Wuhan 430079, People's Republic of China*
[7]*Central South University, Changsha 410083, People's Republic of China*
[8]*China Center of Advanced Science and Technology, Beijing 100190, People's Republic of China*
[9]*China University of Geosciences, Wuhan 430074, People's Republic of China*
[10]*Chung-Ang University, Seoul, 06974, Republic of Korea*
[11]*COMSATS University Islamabad, Lahore Campus, Defence Road, Off Raiwind Road, 54000 Lahore, Pakistan*
[12]*Fudan University, Shanghai 200433, People's Republic of China*
[13]*GSI Helmholtzcentre for Heavy Ion Research GmbH, D-64291 Darmstadt, Germany*
[14]*Guangxi Normal University, Guilin 541004, People's Republic of China*
[15]*Guangxi University, Nanning 530004, People's Republic of China*

[16]*Hangzhou Normal University, Hangzhou 310036, People's Republic of China*
[17]*Hebei University, Baoding 071002, People's Republic of China*
[18]*Helmholtz Institute Mainz, Staudinger Weg 18, D-55099 Mainz, Germany*
[19]*Henan Normal University, Xinxiang 453007, People's Republic of China*
[20]*Henan University, Kaifeng 475004, People's Republic of China*
[21]*Henan University of Science and Technology, Luoyang 471003, People's Republic of China*
[22]*Henan University of Technology, Zhengzhou 450001, People's Republic of China*
[23]*Huangshan College, Huangshan 245000, People's Republic of China*
[24]*Hunan Normal University, Changsha 410081, People's Republic of China*
[25]*Hunan University, Changsha 410082, People's Republic of China*
[26]*Indian Institute of Technology Madras, Chennai 600036, India*
[27]*Indiana University, Bloomington, Indiana 47405, USA*
[28a]*INFN Laboratori Nazionali di Frascati, I-00044 Frascati, Italy*
[28b]*INFN Sezione di Perugia, I-06100 Perugia, Italy*
[28c]*University of Perugia, I-06100 Perugia, Italy*
[29a]*INFN Sezione di Ferrara, I-44122 Ferrara, Italy*
[29b]*University of Ferrara, I-44122 Ferrara, Italy*
[30]*Inner Mongolia University, Hohhot 010021, People's Republic of China*
[31]*Institute of Modern Physics, Lanzhou 730000, People's Republic of China*
[32]*Institute of Physics and Technology, Peace Avenue 54B, Ulaanbaatar 13330, Mongolia*
[33]*Instituto de Alta Investigación, Universidad de Tarapacá, Casilla 7D, Arica 1000000, Chile*
[34]*Jilin University, Changchun 130012, People's Republic of China*
[35]*Johannes Gutenberg University of Mainz, Johann-Joachim-Becher-Weg 45, D-55099 Mainz, Germany*
[36]*Joint Institute for Nuclear Research, 141980 Dubna, Moscow region, Russia*
[37]*Justus-Liebig-Universitaet Giessen, II. Physikalisches Institut, Heinrich-Buff-Ring 16, D-35392 Giessen, Germany*
[38]*Lanzhou University, Lanzhou 730000, People's Republic of China*
[39]*Liaoning Normal University, Dalian 116029, People's Republic of China*
[40]*Liaoning University, Shenyang 110036, People's Republic of China*
[41]*Nanjing Normal University, Nanjing 210023, People's Republic of China*
[42]*Nanjing University, Nanjing 210093, People's Republic of China*
[43]*Nankai University, Tianjin 300071, People's Republic of China*
[44]*National Centre for Nuclear Research, Warsaw 02-093, Poland*
[45]*North China Electric Power University, Beijing 102206, People's Republic of China*
[46]*Peking University, Beijing 100871, People's Republic of China*
[47]*Qufu Normal University, Qufu 273165, People's Republic of China*
[48]*Renmin University of China, Beijing 100872, People's Republic of China*
[49]*Shandong Normal University, Jinan 250014, People's Republic of China*
[50]*Shandong University, Jinan 250100, People's Republic of China*
[51]*Shanghai Jiao Tong University, Shanghai 200240, People's Republic of China*
[52]*Shanxi Normal University, Linfen 041004, People's Republic of China*
[53]*Shanxi University, Taiyuan 030006, People's Republic of China*
[54]*Sichuan University, Chengdu 610064, People's Republic of China*
[55]*Soochow University, Suzhou 215006, People's Republic of China*
[56]*South China Normal University, Guangzhou 510006, People's Republic of China*
[57]*Southeast University, Nanjing 211100, People's Republic of China*
[58]*State Key Laboratory of Particle Detection and Electronics, Beijing 100049, Hefei 230026, People's Republic of China*
[59]*Sun Yat-Sen University, Guangzhou 510275, People's Republic of China*
[60]*Suranaree University of Technology, University Avenue 111, Nakhon Ratchasima 30000, Thailand*
[61]*Tsinghua University, Beijing 100084, People's Republic of China*
[62a]*Turkish Accelerator Center Particle Factory Group, Istinye University, 34010, Istanbul, Turkey*
[62b]*Near East University, Nicosia, North Cyprus, 99138, Mersin 10, Turkey*
[63]*University of Chinese Academy of Sciences, Beijing 100049, People's Republic of China*
[64]*University of Groningen, NL-9747 AA Groningen, The Netherlands*
[65]*University of Hawaii, Honolulu, Hawaii 96822, USA*
[66]*University of Jinan, Jinan 250022, People's Republic of China*
[67]*University of Manchester, Oxford Road, Manchester, M13 9PL, United Kingdom*
[68]*University of Muenster, Wilhelm-Klemm-Strasse 9, 48149 Muenster, Germany*
[69]*University of Oxford, Keble Road, Oxford OX13RH, United Kingdom*

[70]*University of Science and Technology Liaoning, Anshan 114051, People's Republic of China*
[71]*University of Science and Technology of China, Hefei 230026, People's Republic of China*
[72]*University of South China, Hengyang 421001, People's Republic of China*
[73]*University of the Punjab, Lahore-54590, Pakistan*
[74a]*University of Turin and INFN, University of Turin, I-10125 Turin, Italy*
[74b]*University of Eastern Piedmont, I-15121 Alessandria, Italy*
[74c]*INFN, I-10125 Turin, Italy*
[75]*Uppsala University, Box 516, SE-75120 Uppsala, Sweden*
[76]*Wuhan University, Wuhan 430072, People's Republic of China*
[77]*Yantai University, Yantai 264005, People's Republic of China*
[78]*Yunnan University, Kunming 650500, People's Republic of China*
[79]*Zhejiang University, Hangzhou 310027, People's Republic of China*
[80]*Zhengzhou University, Zhengzhou 450001, People's Republic of China*

[a]Deceased.
[b]Also at the Moscow Institute of Physics and Technology, Moscow 141700, Russia.
[c]Also at the Novosibirsk State University, Novosibirsk, 630090, Russia.
[d]Also at the NRC "Kurchatov Institute", PNPI, 188300, Gatchina, Russia.
[e]Also at Goethe University Frankfurt, 60323 Frankfurt am Main, Germany.
[f]Also at Key Laboratory for Particle Physics, Astrophysics and Cosmology, Ministry of Education; Shanghai Key Laboratory for Particle Physics and Cosmology; Institute of Nuclear and Particle Physics, Shanghai 200240, People's Republic of China.
[g]Also at Key Laboratory of Nuclear Physics and Ion-beam Application (MOE) and Institute of Modern Physics, Fudan University, Shanghai 200443, People's Republic of China.
[h]Also at State Key Laboratory of Nuclear Physics and Technology, Peking University, Beijing 100871, People's Republic of China.
[i]Also at School of Physics and Electronics, Hunan University, Changsha 410082, China.
[j]Also at Guangdong Provincial Key Laboratory of Nuclear Science, Institute of Quantum Matter, South China Normal University, Guangzhou 510006, China.
[k]Also at MOE Frontiers Science Center for Rare Isotopes, Lanzhou University, Lanzhou 730000, People's Republic of China.
[l]Also at Lanzhou Center for Theoretical Physics, Lanzhou University, Lanzhou 730000, People's Republic of China.
[m]Also at the Department of Mathematical Sciences, IBA, Karachi 75270, Pakistan.
[n]Also at Ecole Polytechnique Federale de Lausanne (EPFL), CH-1015 Lausanne, Switzerland.
[o]Also at Helmholtz Institute Mainz, Staudinger Weg 18, D-55099 Mainz, Germany.